

## Structures of exotic nuclei from analyses of nucleon-nucleus scattering data.

K. Amos<sup>1</sup>, P. Fraser<sup>1</sup>, D. van der Knijff<sup>1</sup>,  
S. Karataglidis<sup>2</sup>, J. P. Svenne<sup>3</sup>,  
L. Canton<sup>4</sup>, and G. Pisent<sup>4</sup>

<sup>1</sup> *University of Melbourne, Victoria 3010, Australia*

<sup>2</sup> *Rhodes University, Grahamstown 6140, South Africa*

<sup>3</sup> *University of Manitoba, Winnipeg, Manitoba, Canada R3T 2N2*

<sup>4</sup> *I.N.F.N and Università di Padova, Padova I-35131*

### I. INTRODUCTION

An ultimate aim of scattering theory is to probe the structure of nuclei. Data may be taken with electrons, mesons, nucleons, and nuclei as probes, with form factors, cross sections, spin observables being data. There are diverse reactions one might consider (elastic and inelastic scattering and particle exchange reactions are some). But almost all theories rely upon elastic scattering information and require, as input, specifics of a model for the nuclear structure. However, an important requirement in nuclear theory is the phenomenological construction of an interaction Hamiltonian for nucleon-nucleus and/or nucleus-nucleus systems, that is realistic for both bound states and scattering (including resonances). To do so is important for many reasons; theoretical consistency, for evaluation of EM transitions, radiative captures, etc., as required input for cluster-like, three-body calculations of core nucleus-N-N, core-core-N, and core-core-core systems, of systems that are important for current and future experimental researches using radioactive ion beams (RIBs), in nuclear data evaluation for applications such as of radiation safety, nuclear medicine, nuclear astrophysics, and nuclear weapon stewardship. Such remains a ‘holy grail’ and approximate methods are still the practical means

for studies of nuclear structure and reactions.

The real question then is what structure model to use and what reaction theory is appropriate — or what are the ‘horses for courses’?

Consider first what (light mass) nuclear spectra are in general. At low excitations, there are discrete states while at excitations above any giant resonances, there is a continuum of states. Those aspects of a target effect the choice of scattering theory to be used. For low incident energies, discrete states of the target should play significant roles. This means one needs to solve a coupled-channels problem. The MCAS approach [1] was designed to do that. For higher incident energies, however, the continuum is the important feature of the target and there are so many states of the target to effect a response, that an average scheme may be relevant. The  $g$ -folding optical potential model (for elastic scattering) and the DWA for inelastic processes works very well in those cases [2].

With low energy situations, the MCAS method gives spectra of compound nuclei formed by the amalgamation of two separate nuclear clusters. Sub-threshold (bound states) if they exist, as well as resonance states (for energies above the two cluster threshold) can be deduced using it. Those resonances can be narrow or broad. Some of the first type can be identified as bound states embedded in the continuum (BSEC) while broad resonances are characteristic of single particle potential resonances. It has been noted in the literature that

*”The BSEC phenomena can lead to a change in the level density close to the continuum threshold, so such structures will be highly important in the astrophysical capture and knockout reactions contributing to nuclear synthesis in neutron rich stellar environments”.*

For scattering at energies above a few tens of MeV per nucleon, the number of target states to be included in a full MCAS calculation makes evaluation with that scheme

no longer feasible. However, when the energies coincide with a region of high density of states in the target, an alternative approach that has proved very successful is to use  $g$ -folding optical potentials in an analysis of elastic scattering observables, and to use the relative motion wave functions they produce as the distorted waves in a DWA analysis of inelastic scattering data. The underlying two-nucleon (NN)  $g$ -matrices in the generation of the optical potentials are complex, medium and energy dependent and are also used as the transition operator effecting the inelastic transitions. It is important to note that the  $g$ -folding optical potentials are very non-local and that the actual non-locality must be used in evaluations and not approximated by a local equivalent form in these studies. Often, and still to this day, phenomenological, local optical model potentials are used to determine the distorted wave functions of relative motion with the argument that a quality fit to the elastic scattering data justifies use of the associated relative motion wave functions. But such fits only require specification of a suitable set of phase shifts which are determined from the asymptotic properties of the solutions. The credibility of distorted wave functions through the volume of the nucleus cannot be assured thereby. Indeed, it has long been known that those wave functions are too large through the nuclear volume due to inadequate representation of nonlocal effects.

In the next two sections, we present elements of the MCAS and  $g$ -folding methods along with some results of applications to illustrate the flexibility and use of them. Then in Section IV we employ both methods in a study of the spectra of the isotopes of carbon ranging between the drip lines. Another application of the MCAS method, namely to define a spectrum of  $\Lambda$  hypernuclei, is reported in Section V, after which brief concluding remarks are given.

## II. MCAS AND NUCLEON-NUCLEUS SYSTEMS AT LOW AND NEGATIVE ENERGIES

In brief, the MCAS approach is based upon using sturmian functions (Weinberg states) as a basis set to expand the chosen interaction potentials. Each interaction matrix then has the form of a sum of separable interactions. The analytic properties of the  $S$  matrix from a separable Schrödinger potential gives the means by which a full algebraic solution of the multichannel scattering problem can be realized. All details of the MCAS theory have been published [1] and so only salient features are repeated herein. Consider a coupled-channel system for each allowed scattering spin-parity  $J^\pi$ . With the MCAS method, one solves the Lippmann-Schwinger (LS) integral equations in momentum space,

$$T_{cc'}(p, q; E) = V_{cc'}(p, q) + \frac{2\mu}{\hbar^2} \left[ \sum_{c''=1}^{\text{open}} \int_0^\infty \frac{V_{cc''}(p, x) T_{c''c'}(x, q; E)}{k_{c''}^2 - x^2 + i\epsilon} x^2 dx - \sum_{c''=1}^{\text{closed}} \int_0^\infty \frac{V_{cc''}(p, x) T_{c''c'}(x, q; E)}{h_{c''}^2 + x^2} x^2 dx \right],$$

where the index  $c$  denotes the quantum numbers that identify each channel uniquely. Such requires specification of potential matrices  $V_{cc'}^{(J^\pi)}(p, q)$ . The open and closed channels have channel wave numbers  $k_c$  and  $h_c$  for  $E > \epsilon_c$  and  $E < \epsilon_c$  respectively.  $\mu$  is the reduced mass. Solutions of these LS equations are sought using expansions of the potential matrix elements in (finite) sums of energy-independent separable terms,

$$V_{cc'}(p, q) \sim \sum_{n=1}^N \chi_{cn}(p) \eta_n^{-1} \chi_{c'n}(q).$$

The key to the method is the choice of the expansion form factors  $\chi_{cn}(q)$ . Optimal ones have been found from the sturmian functions that are determined from the actual (coordinate space) model interaction  $V_{cc'}(r)$  initially

chosen to describe the coupled-channel problem.

The link between the multichannel  $T$ - and the scattering ( $S$ -) matrices involves a Green's function matrix,

$$(G_0)_{nn'} = \frac{2\mu}{\hbar^2} \left[ \sum_{c=1}^{\text{open}} \int_0^\infty \frac{\chi_{cn}(x) \chi_{cn'}(x)}{k_c^2 - x^2 + i\epsilon} x^2 dx - \sum_{c=1}^{\text{closed}} \int_0^\infty \frac{\chi_{cn}(x) \chi_{cn'}(x)}{h_c^2 + x^2} x^2 dx \right],$$

where  $(\eta)_{nn'}$  is a diagonal eigenvalue matrix ( $\eta_n \delta_{nn'}$ ). The bound states of the compound system are defined by the zeros of the matrix determinant for energy  $E < 0$ . They link to the zeros of  $\{\boldsymbol{\eta} - \mathbf{G}_0\}$  when all channels in the above are closed.

Elastic scattering observables follow from the on-shell properties ( $k_1 = k_1' = k$ ) of the scattering matrices. For the elastic scattering of neutrons (spin  $\frac{1}{2}$ ) from spin zero targets  $c = c' = 1$ , and  $S_{11} \equiv S_\ell^J = S_\ell^{(\pm)}$  are

$$S_{11} = 1 - i\pi \frac{2\mu k}{\hbar^2} \sum_{nn'=1}^M \chi_{1n}(k) \times \frac{1}{\sqrt{\eta_n}} \left[ \left( \mathbf{1} - \boldsymbol{\eta}^{-\frac{1}{2}} \mathbf{G}_0 \boldsymbol{\eta}^{-\frac{1}{2}} \right)^{-1} \right]_{nn'} \frac{1}{\sqrt{\eta_{n'}}} \chi_{1n'}(k).$$

Diagonalization of the complex-symmetric matrix,

$$\sum_{n'=1}^N \eta_n^{-\frac{1}{2}} [\mathbf{G}_0]_{nn'} \eta_{n'}^{-\frac{1}{2}} \tilde{Q}_{n'r} = \zeta_r \tilde{Q}_{nr},$$

establishes the evolution of the complex eigenvalues  $\zeta_r$  with respect to energy. Resonant behaviour occurs when an eigenvalue  $\zeta_r$  crosses the unit circle in the Gauss plane. The energy at which such occurs is the resonance centroid. It is evident that the elastic channel  $S$  matrix has a pole structure at the corresponding energy where one of these eigenvalues approach unity, since

$$\left[ \left( \mathbf{1} - \boldsymbol{\eta}^{-\frac{1}{2}} \mathbf{G}_0 \boldsymbol{\eta}^{-\frac{1}{2}} \right)^{-1} \right]_{nn'} = \sum_{r=1}^N \tilde{Q}_{nr} \frac{1}{1 - \zeta_r} \tilde{Q}_{n'r}.$$

While the required starting matrix of potentials within the MCAS method may be constructed from any model of nuclear structure, to date we have used just simple collective models to define those potentials with deformation taken to second order. Also, to date the only the first few (3 to 5) low lying states of the target nucleus have been used to form the channel couplings.

### III. $g$ -FOLDING OPTICAL POTENTIALS AND THE DWA

To predict the differential cross sections for both elastic and inelastic scattering from the Carbon isotopes we use the microscopic  $g$ -folding model of the Melbourne group [2]. That model begins with the  $NN$   $g$  matrices for the interaction of a nucleon with infinite nuclear matter. Starting with the Bonn-B free  $NN$  interaction [3], those  $g$  matrices are solutions of BBG (Brueckner-Bethe-Goldstone) equations in infinite nuclear matter, *viz.*

$$g(\mathbf{q}', \mathbf{q}; K) = V(\mathbf{q}', \mathbf{q}) + \int V(\mathbf{q}', \mathbf{k}') [\mathcal{P}] g(\mathbf{k}', \mathbf{q}; \mathbf{K}) d\mathbf{k}',$$

$$\text{where } \mathcal{P} = \frac{Q(\mathbf{k}', \mathbf{K}; k_f)}{[E(\mathbf{k}, \mathbf{K}) - E(\mathbf{k}', \mathbf{K})]},$$

in which both Pauli blocking of states and an average background mean field in which the nucleons move, leading to  $g$  matrices that are complex, energy dependent, medium (density) dependent, and nonlocal in that the solutions for different partial waves reflect tensorial character. Such can be, and have been, used directly in momentum space evaluations of  $NA$  (elastic) scattering [4], but we prefer to analyze data using a coordinate space representation. For this, and to make use of the program suite DWBA98 [5], the  $g$  matrices must be mapped, via a double Bessel transform to equivalent forms in coordinate space. Folding those effective interactions,

$g_{\text{eff}}(0, 1)$  with the density-matrices of the target then yields a complex, nonlocal, density-dependent, nucleon-nucleus ( $NA$ ) optical potential from which the elastic scattering observables are obtained. Full details of this prescription can be found in the review article [2].

Inelastic nucleon scattering is calculated within the Distorted-Wave-Approximation (DWA) using the effective coordinate space  $g$ -matrices ( $g_{\text{eff}}(0, 1)$ ) as the transition operator. Again full details are to be found in the review [2]. The transition amplitude is given by

$$T_{J_f J_i}^{M_f M_i \nu' \nu}(\theta) = \left\langle \chi_{\nu'}^{(-)} \left| \langle \Psi_{J_f M_f} | A g_{\text{eff}} \mathcal{A}_{01} \{ |\chi_{\nu}^{(+)} \rangle | \Psi_{J_i M_i} \rangle \right. \right\rangle,$$

where  $\chi^{(\pm)}$  are distorted wave functions for an incident and an emergent nucleon respectively. Those wave functions are generated from  $g$ -folding optical potentials. Coordinates 0 and 1 are those of the projectile and a chosen struck bound state nucleon, respectively. By using a co-factor expansion of the target wave function one obtains

$$T_{J_f J_i}^{M_f M_i \nu' \nu}(\theta) = \sum_{\alpha_k, m_i} \sum_{JM} \frac{(-1)^{j_1 - m_1}}{\sqrt{2J_f + 1}} \langle j_2 m_2 j_1 - m_1 | J_f M_f \rangle \langle J_i M_i J M | J_f M_f \rangle \left\langle J_f \left\| [a_{\alpha_2}^\dagger \times \tilde{a}_{\alpha_1}]^J \right\| J_i \right\rangle \left\langle \chi_{\nu'}^{(-)} \left| \langle \varphi_{\alpha_2} | A g_{\text{eff}} \mathcal{A}_{01} \{ |\chi_{\nu}^{(+)}(0) \rangle | \varphi_{\alpha_1}(1) \rangle \right. \right\rangle$$

for an angular momentum transfer  $J$ , and  $\alpha$  denotes the set of single-particle quantum numbers  $\{n, l, j, m_\tau\}$ , where  $\tau$  is the nucleon isospin. Thus the scattering amplitudes are weighted sums of two nucleon amplitudes; the weights being transition one-body-density-matrix-elements, OBDME,

$$S_{\alpha_1 \alpha_2 I}^{J_i J_f} = \left\langle J_f \left\| [a_{\alpha_2}^\dagger \times \tilde{a}_{\alpha_1}]^J \right\| J_i \right\rangle,$$

and which are to be defined from whatever model of nuclear structure is used. With

the  $g$ -folding potentials defining the distorted waves, and the  $g_{\text{eff}}$  being the transition operator, in the DWA, the problem reduces to one of specifying the structure of the target. For this study we have used two different models. The first is the Skyrme-Hartree-Fock (SHF) model of Brown [6]. With that model and using the SKX interaction, ground state densities and single nucleon wave functions have been defined. However, as the SHF model cannot provide information on the spectrum of the target, we have also used a  $(0 + 2)\hbar\omega$  shell model (SM) with which we have specified the transition densities necessary in calculation of inelastic scattering. Note that for  $^{10,12,14}\text{C}$ , this SM is complete while for  $^{16}\text{C}$  and  $^{18}\text{C}$  the space is truncated, excluding the  $0g1d2s$  shell required for a complete evaluation of  $1p-1h$ ,  $2\hbar\omega$  excitations from the  $1s0d$  shell. Calculations have been made using the OXBASH shell model program [7] with the WBP interaction of Warburton and Brown [8] suitably corrected for center-of-mass effects. With that model the ground state wave functions for  $^{10}\text{C}$ ,  $^{12}\text{C}$  and  $^{14}\text{C}$  are

$$\begin{aligned} |^{10}\text{C}\rangle &= 92.4\% |0\hbar\omega\rangle + 7.6\% |2\hbar\omega\rangle \\ |^{12}\text{C}\rangle &= 87.0\% |0\hbar\omega\rangle + 13.0\% |2\hbar\omega\rangle \\ |^{14}\text{C}\rangle &= 84.9\% |0\hbar\omega\rangle + 15.1\% |2\hbar\omega\rangle, \end{aligned}$$

while the states in  $^{16}\text{C}$  and  $^{18}\text{C}$  are purely  $2\hbar\omega$  in character.

Table I contains the SM predictions of the energies, and the  $B(E2)$  values for excitation, of the  $2^+$  states in the even mass C isotopes. The polarization charge required to match theory to measured  $B(E2)$  values are also given. Most data were taken from ref. [9] and they are supplemented with data on  $^{16}\text{C}$  from refs. [10, 11] and on  $^{18}\text{C}$  from ref. [12]. The agreement between the results of the SM calculations with data is quite good. Note that the energy of the  $2^+$  state in  $^{14}\text{C}$  is much larger than the other isotopes. However, the  $2^+$  assignment for the 1.62 MeV state in  $^{18}\text{C}$  is only tentative [9]. It is notable that the polarization charges required to match the observed values of the  $B(E2)$ , save for the

TABLE I: Shell model  $B(E2; 0^+ \rightarrow 2^+)$  values.

Nucleus	Ex (exp) MeV	$B(E2)$ $e^2\text{fm}^4$	$B(E2)_{\text{exp}}$ $e^2\text{fm}^4$	$e_{\text{pol}}$ e
$^{12}\text{C}$	4.29 (4.43)	17.90	40 (3)	0.248
$^{14}\text{C}$	6.33 (7.01)	15.90	19 (3)	0.069
	7.14	2.90		
$^{16}\text{C}$	2.33 (1.77)	1.68	3.1 (6)	0.053
	2.39	2.63		
$^{18}\text{C}$	2.05 (1.59)	4.40	4.3 (1.0)	0

case of  $^{12}\text{C}$  are quite small. In view of past and recent studies and the correlations found therein [2, 13], such gives confidence that use of these structures later will predict proton cross sections for inelastic excitation of those  $2^+$  states that will be found experimentally.

#### IV. STUDIES OF THE ISOTOPES OF CARBON USING NUCLEON-CARBON INTERACTIONS

There has been much speculation concerning the possible melting or changing of the shell structure of nuclei as one moves away from the valley of stability. With light mass nuclei there are indications of possible changes in the magic numbers. Around  $^{32}\text{Mg}$  such lead an ‘‘island of inversion’’ [14]. In structure calculations, such variations are influenced by three-body forces [15], as well as by changes in the monopole term of the Hamiltonian. The latter has been shown to cause changes to the single particle energies as one approaches the drip lines. So, in theory, there are reasons to expect new magic numbers in nuclei off of the stability line [16].

Were there to be such an extreme change in the shell structure in nuclei as that system becomes neutron or proton rich away from stability, means by which to identify that is required. For even mass nuclei, one way is to consider the energy of the first  $2^+$  state systematically about a suspected closed shell [17]. We suggest that, besides expected

signatures in the spectrum, the cross sections from inelastic scattering of the (radioactive) isotopes or isotones, as radioactive ion beams (RIBs), around the closed shell nucleus from hydrogen targets will reveal a definite variation with mass.

The even mass Carbon isotopes provide a set of nuclei with which one may observe a trend from the proton ( $^{10}\text{C}$ ) to the neutron ( $^{18}\text{C}$ ) drip lines. They also span a known neutron shell closure  $^{14}\text{C}$  as evident from their low lying spectra. In the spectra of  $^{10,12,16,18}\text{C}$  the first excited state has spin-parity  $2^+$  and excitation energies of 3.35, 4.43, 1.77, and 1.62 MeV respectively. In contrast, in the spectrum of  $^{14}\text{C}$ , the first excited state, with spin-parity  $1^-$  is associated with a cluster of states in the range 6 to 7 MeV. Spin-parities of those states are in sequence  $1^-, 0^+, 3^-, 0^-$  and then  $2^+$ . Thus these nuclei are an excellent set with which to show any signature of shell closure with scattering data. Of course there are other properties one can consider to note shell closures, for example the  $B(E2)$  value [18].

Herein, we look to scattering to investigate a means by which shell closures and crossing may be identified. In particular, we consider proton scattering at intermediate energies (E) which, by inverse kinematics, equates to RIB scattering (E per nucleon) from hydrogen targets. At these energies, the nucleon-nucleon ( $NN$ ) potential is dominated by the  $V_{pn}$  component interaction [2] and so proton scattering primarily, though not exclusively, probes the neutron density in a nucleus. By symmetry, neutron scattering primarily is a probe of the proton distribution in the nucleus.

As noted, the neutron shell closure in the Carbon isotopes occurs at  $^{14}\text{C}$ , with a closed  $0p$ -shell. There is closure of the  $0p_{3/2}$  shell in  $^{12}\text{C}$ , but that is not a purely closed sub-shell as there are significant  $2p$ - $2h$  terms in the wave function. We consider inelastic scattering leading to the first  $2^+$  state in each isotope, as there may be a significant change

in the cross section shape at the shell closure consistent with the change in the spectrum. Changes are expected to occur in both the elastic and the inelastic scattering around the  $^{14}\text{C}$  results. However, to establish such requires a scattering theory that is predictive, i.e. not subject to parameter adjustment.

### A. Using MCAS and the spectra of odd-mass isotopes

The first application of the MCAS method was to find the spectrum of  $^{13}\text{C}$  from calculations of the  $n+^{12}\text{C}$  system. Details are given in Ref. [1]. We simply note here that, treating the problem as a three target state coupling one, using a collective rotor model specification of the interaction matrix of potentials, accounting for the Pauli blocking of the occupied nucleon orbits in the target, and using the resonance finding methodology, gave a very credible spectrum for  $^{13}\text{C}$  with one to one matching of all known states to  $\sim 10$  MeV excitation.

More recently [19], the spectrum of  $^{15}\text{C}$  treating it from the  $n+^{14}\text{C}$  system was determined. The result is shown on the left of Fig. 1. The energy scale is that for a neutron on  $^{14}\text{C}$  and the states of  $^{14}\text{C}$  shown were used in the MCAS evaluations. An interaction matrix was found that gave the spectrum of  $^{15}\text{C}$  labelled by ‘MCAS’ which is compared with the known spectrum (‘EXP.’). The states identified by twice their spin and their parity match very well especially given that the calculated width of the  $\frac{3}{2}^+$  resonance is indicated by the dashed lines is quite large.

That nuclear interaction then was used to study the  $p+^{14}\text{O}$  system given that such is the mirror isospin of  $n+^{14}\text{C}$ . Only a Coulomb interaction was added. The resulting spectrum made  $^{15}\text{F}$  particle unstable, as it is, with a  $\frac{1}{2}^+$  resonant ground state. Low energy scattering experiments of  $^{14}\text{O}$  ions from hydrogen targets gave cross sections as shown in the right side of Fig. 1. The cross section displayed by the solid curve is that obtained

from the MCAS evaluation. It is of note that the theory also expects resonance behaviour at slightly higher incident energies than used to date.

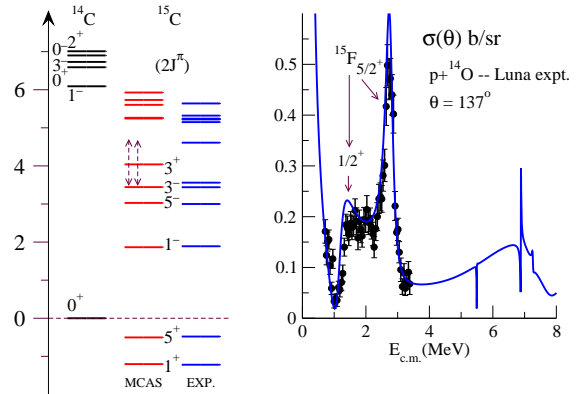


FIG. 1: (Color online.) The low excitation spectrum of  $^{15}\text{C}$  relative to the  $n+^{14}\text{C}$  threshold and a cross section from  $^{14}\text{O}$  ions scattering from hydrogen.

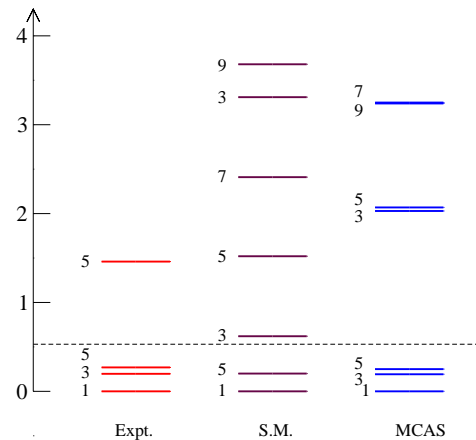


FIG. 2: (Color online.) The low excitation spectrum of  $^{19}\text{C}$ . The data are compared with the results of a  $2\hbar\omega$  SM calculation (SM) and with a spectrum found using the MCAS approach. The dashed line indicates the  $n+^{18}\text{C}$  threshold, while the numeral identifying each state is  $2J$ .

In Fig. 2 the currently known states [20] in the spectrum of  $^{19}\text{C}$  are compared with the low excitation spectra for this nucleus

determined from a SM calculation and with that found from the coupled-channel solutions (MCAS) based upon a two-state, collective, model for the  $n+^{18}\text{C}$  system. The prolate deformation required was quite important to get the three low lying states. The variation of the spectrum found by varying the deformation parameter  $\beta_2$  is displayed in Fig. 3. The excitation energies of the states all vary regularly as the deformation increases, either for prolate (positive  $\beta_2$ ) or oblate (negative  $\beta_2$ ) character. Two states stand out as being dominantly the coupling of a single neutron to the ground state of  $^{18}\text{C}$ . They are denoted by the filled circles (lowest set) being the ground state of  $^{19}\text{C}$  formed (when  $\beta_2 = 0$ ) with a  $1s_{1/2}$ -neutron, and by the filled triangles being a state formed (when  $\beta_2 = 0$ ) with a  $5/2^+$ -neutron. These states vary with deformation noticeably more slowly than the others. That is so especially for the ground state reflecting that the prime admixing component (the  $\left[0d_{5/2} \otimes 2^+\right]_{1/2}$ ) lies above 4 MeV in the unperturbed spectrum. But it is important to note that the deformation coupling mixes all basic states of given spin-parity to form the resultant ones in the spectrum of  $^{19}\text{C}$ . From this plot it is also clear that our coupled-channel calculations require a strong deformation  $\sim 0.4$  to obtain three states of the appropriate spin-parity lying below the neutron- $^{18}\text{C}$  threshold and still retaining a one-neutron separation energy of  $\sim 0.53$  MeV.

The spectrum of  $^{17}\text{C}$  has been studied in the same way and similar results found to those for  $^{19}\text{C}$ .

### B. Using $g$ -folding optical potentials

The differential cross sections for the elastic scattering of 100 MeV protons from  $^{10-18}\text{C}$  using the shell occupancies and single particle wave functions obtained by using the shell model, are displayed in Fig. 4. For the shell model, an oscillator parameter of 1.65 fm

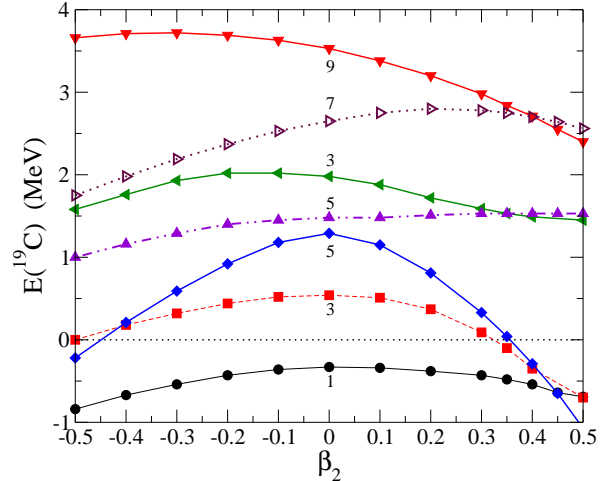


FIG. 3: (Color online.) The low excitation spectrum of  $^{19}\text{C}$  calculated with variation of the deformation  $\beta_2$ .

was used to specify the single-particle wave functions. There is a steady increase in the

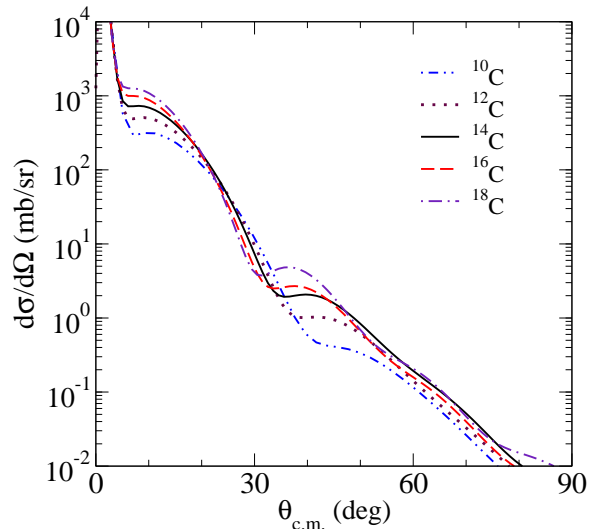


FIG. 4: (Color online.) The differential cross sections for the elastic scattering of 100 MeV protons from the even isotopes of Carbon when their structure was obtained from the shell model.

cross section with angle indicating an increasing rms radius with mass. Beyond the first diffraction minimum the cross sections from  $^{10}\text{C}$  and  $^{12}\text{C}$  are significantly reduced com-

pared to the other isotopes. That indicates the lack of  $0p$ -shell strength in the density, as  $^{14,16,18}\text{C}$  all have a closed  $0p$  neutron shell.

Consider next, the inelastic scattering to the first  $2^+$  state in each nucleus. Using the shell model structures to define the transition OBDME, the differential cross sections for the inelastic scattering of 100 MeV protons to the  $2^+$  state in each nucleus are displayed in Fig. 5. Here, the differential cross

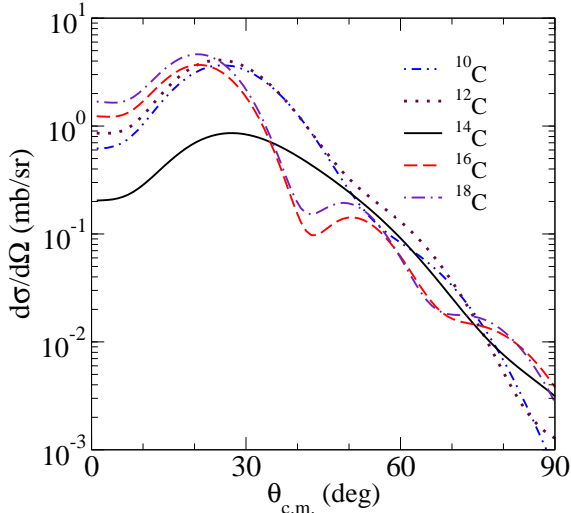


FIG. 5: (Color online.) The differential cross sections for the inelastic scattering of 100 MeV protons to the  $2^+$  states in  $^{10-18}\text{C}$ , as obtained from the shell model calculations.

sections from  $^{10,12}\text{C}$  and  $^{16,18}\text{C}$  while comparable in magnitude are most distinctly different in shape. That indicates the change in the density with the introduction of the  $sd$ -shell neutrons in  $^{16,18}\text{C}$ . Most striking is the reduction in strength of the differential cross section from scattering to the  $2^+$  state in  $^{14}\text{C}$ . This reduction is an order of magnitude at  $0^\circ$  decreasing to a factor of 6 at  $20^\circ$ . As the neutron shell is closed in  $^{14}\text{C}$ , for this nucleus, there is very little neutron strength in the transition density. That translates into a reduction in the inelastic cross section compared to those from excitations of the  $2^+$  states in the other isotopes.

In a recent paper, Satou *et al.* [20] report data from the inelastic scattering of  $^{17,19}\text{C}$

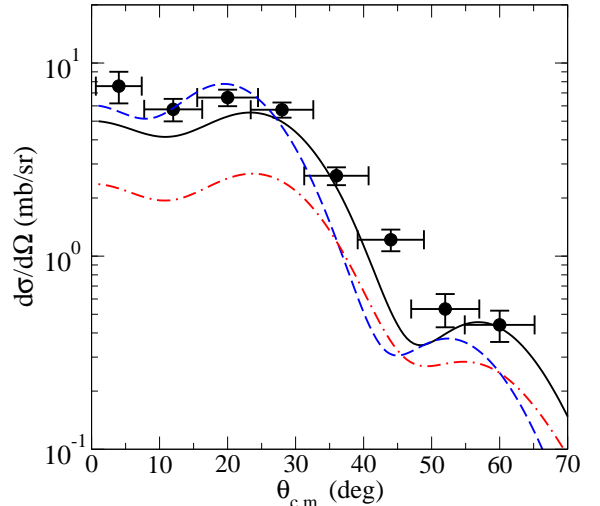


FIG. 6: (Color online.) The differential cross sections for the inelastic scattering of 70 MeV protons from  $^{19}\text{C}$  leading to the state at 1.46 MeV excitation.

ions from a hydrogen target. Differential cross sections from the scattering of 70 MeV ions leading to states at excitation energies of 2.2 and 3.05 MeV in  $^{17}\text{C}$  and to the 1.46 MeV excited state in  $^{19}\text{C}$  were presented. For illustration only the data from the excitation of the 1.46 MeV state in  $^{19}\text{C}$  are considered herein. They are shown in Fig. 6. There are three evaluations with which these data are compared. Those depicted by the solid and long-dashed curves were made assuming that the ground state had a spin-parity of  $\frac{1}{2}^+$ . Both results are dominated by  $L = 2$  angular momentum transfer. The solid (dashed) curve is the result found using oscillator (Woods-Saxon) functions for the single-nucleon bound-state wave functions that reflect a neutron skin (halo-like) property to the density. The result depicted by the dot-dashed curve, was found using the oscillator wave functions but on assuming that the ground state had a spin-parity of  $\frac{5}{2}^+$ . These results indicate that the ground state of  $^{19}\text{C}$  has indeed the  $\frac{1}{2}^+$  assignment as has been suggested [20], but that it may have a neu-

tron skin rather than a neutron halo.

## V. MCAS AND HYPERNUCLEI

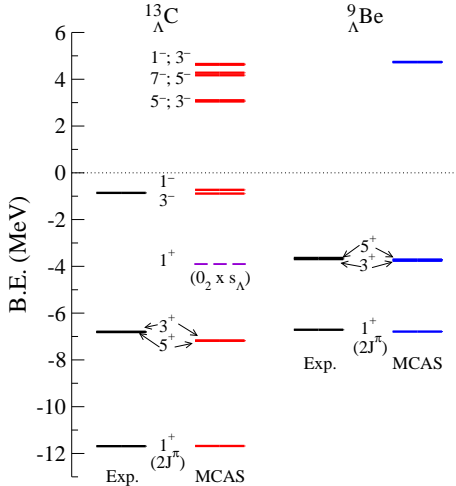


FIG. 7: (Color online.) The spectra of  $^{13}_{\Lambda}\text{C}$  and of  $^9_{\Lambda}\text{Be}$  evaluated using MCAS compared with known states.

Recently the MCAS scheme has been used to study the spectra of hypernuclei. Since the  $\Lambda^0$  particle is a baryon with spin  $\frac{1}{2}$  and a rest mass  $1115.6 \text{ MeV}/c^2$  ( $c/f$  the neutron rest mass is  $940 \text{ MeV}/c^2$ ), MCAS evaluations of  $\Lambda$ -Nucleus systems is very similar to those of neutron-nucleus systems but without any problem of the Pauli principle blocking states. Hypernuclear systems are of some interest in that fine splittings in the hypernuclear spectra link closely to characteristics in the  $\Lambda$ -nucleon interaction. Also, since the hyperon is not restricted by the Pauli principle in the nuclear medium, it can act as a 'tag' to study systems that have excess neutrons, e.g.  $^{48}\text{Ca}$ . With the current MCAS, one can analyse both bound and resonant spectra for (light mass)  $\lambda$ -hypernuclei, to support and interpret experimental investigations.

To illustrate, using nucleon-nucleus interactions scaled as has been done in past studies, *viz.* the central strengths by  $\frac{2}{3}$ , the spin-orbit strengths by an order of magnitude, and

the radii 15 - 20 % smaller, the spectra of  $^{13}_{\Lambda}\text{C}$  and  $^9_{\Lambda}\text{Be}$  were found that are compared with known states of those systems in Fig. 7.

## VI. CONCLUSIONS

The spectra of light mass nuclei show bound and resonant states that are distinct. Likewise low energy cross sections from the collision of nucleons with a (light mass) nucleus shows sharp, as well as broad, resonances lying upon a smooth, energy-dependent background. Those resonances correlate to states in the discrete spectrum of the target. To interpret spectra and such low energy scattering data, the MCAS approach has proved a most effective means to find solutions of the coupled Lippmann-Schwinger equations that define the problems. With isospin symmetry assumed, the method gives spectra for nuclei that are at or beyond the proton drip line. A new application of MCAS, to specify the spectra of  $\Lambda$  hypernuclei was shown as well.

For higher energy nucleon-nucleus scattering data, the  $g$ -folding and DWA approaches are pertinent. Using them, we have found that the cross sections from inelastic scattering may be used to identify shell closure. For the nucleus in which that shell closure occurs, the transition density can be markedly reduced from similar transition cross sections in neighbouring isotopes. Beyond the shell closure the change in the density effected by the introduction of higher-order shells is also significant. These two points together are indicative of the major shell closure. While the transition may be investigated with zero-momentum transfer observables, such as  $B(E1)$  values, one may only ascertain the change in the density with data from scattering experiments that probe the density at finite momentum transfer values. But experimental investigation of inelastic scattering must also take elastic scattering data to interpret correctly the underlying optical potentials involved [21].

- 
- [1] K. Amos, L. Canton, G. Pisent, J. P. Svenne, and D. van der Knijff, Nucl. Phys. **A728**, 65 (2003).
- [2] K. Amos, P. J. Dortmans, H. V. von Geramb, S. Karataglidis, and J. Raynal, Adv. Nucl. Phys. **25**, 275 (2000).
- [3] R. Machleidt, K. Holinde, and C. Elster, Phys. Rep. **149**, 1 (1987).
- [4] H. F. Arellano, F. A. Brieva, M. Sander, and H. V. von Geramb, Phys. Rev. C **54**, 2570 (1996).
- [5] J. Raynal (1998), computer program DWBA98, NEA 1209/05.
- [6] B. A. Brown, Phys. Rev. C **58**, 220 (1998).
- [7] OXBASH-MSU (the Oxford-Buenos-Aries-Michigan State University shell model code). A. Etchegoyen, W.D.M. Rae, and N.S. Godwin (MSU version by B.A. Brown, 1986); B.A. Brown, A. Etchegoyen, and W.D.M. Rae, MSUCL Report Number 524 (1986).
- [8] E. K. Warburton and B. A. Brown, Phys. Rev. C **46**, 923 (1992).
- [9] TUNL Nuclear Data Evaluation, <http://www.tunl.duke.edu/nucldata/>.
- [10] N. Imai et al., Phys. Rev. Lett. **92**, 062501 (2004).
- [11] Z. Elekes et al., Phys. Letts. **B 5506**, 34 (2004).
- [12] H. J. Ong et al. (2007), arXiv: nucl-ex/0711.4062.
- [13] K. Amos, S. Karataglidis, and Y. J. Kim (2008), arXiv: nucl-th/0801.1529.
- [14] E. K. Warburton, J. A. Becker, and B. A. Brown, Phys. Rev. C **41**, 1147 (1990).
- [15] S. C. Pieper, K. Varga, and R. B. Wiringa, Phys. Rev. C **66**, 044310 (2002).
- [16] T. Otsuka, R. Fujimoto, Y. Utsuno, B. A. Brown, M. Honma, and T. Mizusaki, Phys. Rev. Lett. **87**, 082502 (2001).
- [17] J. I. Prisciandaro et al., Phys. Lett. **B510**, 17 (2001).
- [18] S. Karataglidis, B. A. Brown, K. Amos, and P. J. Dortmans, Phys. Rev. C **55**, 2826 (1997).
- [19] L. Canton, G. Pisent, J. P. Svenne, K. Amos, and S. Karataglidis, Phys. Rev. Lett **96**, 072502 (2006).
- [20] Y. Satou et al., Phys. Letts. **B660**, 320 (2008).
- [21] K. Amos, W. A. Richter, S. Karataglidis, and B. A. Brown, Phys. Rev. Lett. **96**, 032503 (2006).